1 June 2001

Chemical Physics Letters 340 (2001) 267–274

CHEMICAL PHYSICS LETTERS

www.elsevier.nl/locate/cplett

Solute–solvent interactions: two-dimensional ultrafast infrared vibrational echo experiments

David E. Thompson, K.A. Merchant, M.D. Fayer *

Department of Chemistry, Stanford University, Stanford, CA 94305, USA

Received 14 March 2001; in final form 11 April 2001

Abstract

Two-dimensional (time–frequency) ultrafast IR vibrational echo experiments were used to investigate solute–solvent interactions in solution. The experiments were performed on symmetric (S) and antisymmetric (A) CO stretching modes of (acetylacetonato) dicarbonylrhodium(I) in dibutylphthalate (DBP) at 150 K. The two-dimensional (2D) spectrum displays quantum beats at the nominal frequency difference between the S and A modes. However, as the observation wavelength is moved to higher energy, the quantum beat frequency decreases. The change in frequency is related to the nature of the solute–solvent interactions. Model calculations indicate that interactions with the solvent result in CO local mode frequencies that are strongly correlated.

1. Introduction

The structure and dynamics of a molecule can be strongly influenced by interactions with a surrounding solvent. The nature of solute–solvent interactions is an important problem that has ramifications for many chemical and biological processes. In going from the gas phase to a condensed matter environment, vibrational energies change. The energy shifts are observable in infrared (IR) absorption spectra. Such shifts demonstrate that the structure of a molecule is influenced by interactions with a solvent, but, in general, the spectrum alone cannot be used to determine the character of the solute–solvent interactions. Time-dependent IR experiments, particularly optical coherence experiments, such as the ultrafast vibrational echo, can be used to investigate solute–solvent vibrational dynamics [1–8]. However, the one-dimensional (1D) vibrational echo experiment has limits on the extent of the information that it can provide. Methods are needed that can provide direct information on how a solvent modifies a solute's structural degrees of freedom.

In this Letter, ultrafast IR 2D (time–frequency) vibrational echo experiments are described that explore the manner in which a solute interacts with a solvent. 2D spectrally resolved ultrafast vibrational echo spectroscopy [9] is an addition to an increasing collection of new 2D ultrafast IR spectroscopic methods [5,6,10–15]. The experiments are used to study intermolecular interactions of (acetylacetonato)dicarbonylrhodium(I) ($Rh(CO)_2$ acac) in a solid solution of dibutylphthalate (DBP) [9,16,17]. $Rh(CO)_2$acac has two 'local' oscillators that provide a test bed for the examination of the interactions of distinct parts of a molecule with a solvent. A solid glassy solvent provides an

* Corresponding author. Fax: +1-650-723-4817.
E-mail address: fayer@fayerlab.stanford.edu (M.D. Fayer).

0009-2614/01/$ - see front matter
PII: S0009-2614(01)00432-8

inhomogeneous environment that makes it possible to study how different local environments in a single solvent act on a molecule.

The experiments were conducted on the symmetric (S) and antisymmetric (A) CO stretching modes of $Rh(CO)_2acac$ at $\sim$2000 cm^{-1}. The 2D vibrational echo spectrum (VES) is obtained by spectrally resolving the vibrational echo pulse with a monochromator. The 2D spectrum records the vibrational echo as a function of the detection frequency and the time-delay (τ) between excitation pulses. The time-structure on the vibrational echo pulse contains information about the molecular oscillator/solvent system. Spectrally resolving the vibrational echo pulse Fourier transforms the pulse from the time-domain to the frequency-domain. By spectrally resolving the ultrafast vibrational echo and obtaining a 2D VES, the time-resolution of the short pulses is preserved, the nature of the signal can be more readily elucidated, and additional information can be obtained.

Analysis of the quantum beats that appear in the data provides insights into solute–solvent interactions. The frequency of the S/A quantum beats varies for different observation wavelengths across the $v = 0$–1 inhomogeneous lines. Inhomogeneous broadening and its influence on the quantum beat frequency are discussed in terms of the CO local oscillator energies, their coupling to the solvent, and the coupling between the local oscillators that is responsible for the S and A modes. Analysis of the data indicates that the coupling of the two CO local oscillators to the solvent is highly correlated.

2. Experimental

The 180 fs (FWHM) IR pulses used in the experiments were generated at a 1 kHz repetition rate with a bandwidth (FWHM) of 90 cm^{-1}. The autocorrelation and the spectrum of the pulses are both close to Gaussian in shape with a time-bandwidth product of 0.49. The pulses were produced using an optical parametric amplifier (BBO and $AgGaS_2$) pumped by a regeneratively amplified Ti:Sapphire system. The OPA was tuned to fix the center wavelength of the infrared pulses at $\sim$2045 cm^{-1}, approximately midway between the S (2082 cm^{-1}) and the A (2010 cm^{-1}) absorption bands.

The DBP and $Rh(CO)_2acac$ were obtained from Aldrich. The DBP was distilled to eliminate dissolved water and the $Rh(CO)_2acac$ was handled carefully in a glove box to minimize exposure to air. The sample was contained in a 400 μm copper cell with CaF_2 windows. The cell was mounted on a continuous flow cryostat and cooled to 150 K. Sample temperature was monitored with a silicon diode thermometer attached to one of the CaF_2 windows.

The vibrational echo signal, generated in the $2k_2$–k_1 direction, was dispersed by a 210 line/mm grating in a 1 m monochromator. A mercury cadmium telluride detector at the monochromator exit slit monitored the vibrational echo signal intensity. At each wavelength, a vibrational echo decay was collected as a function of τ using 34 fs steps near $\tau = 0$ and 340 fs steps farther out. Between delay line scans, the monochromator was stepped 2 cm^{-1}. The combined data yield the A and S 2D vibrational echo spectra.

3. Results and discussion

Fig. 1 displays 2D vibrational echo spectra that span the full range of wavelengths of the S and A bands. The inset on the left shows the absorption spectrum. Note that the absorption spectrum has substantial solvent features that are not present in the VES spectrum [10,11]. The solvent absorptions do, however, modify the VES spectrum by changing the interaction amplitude as a function of wavelength [11,18]. The S and A VES features are considerably broader than the corresponding linear absorption bands; the increase in breadth comes almost completely on the red side of the absorption center frequencies. The lower VES shows a rotated view of the A and S bands. The lower VES is shown from the blue side while the upper spectrum is shown from the red side. The inset on the right displays the time-dependence at a single monochromator position on the blue side of the S line (2081 cm^{-1}).

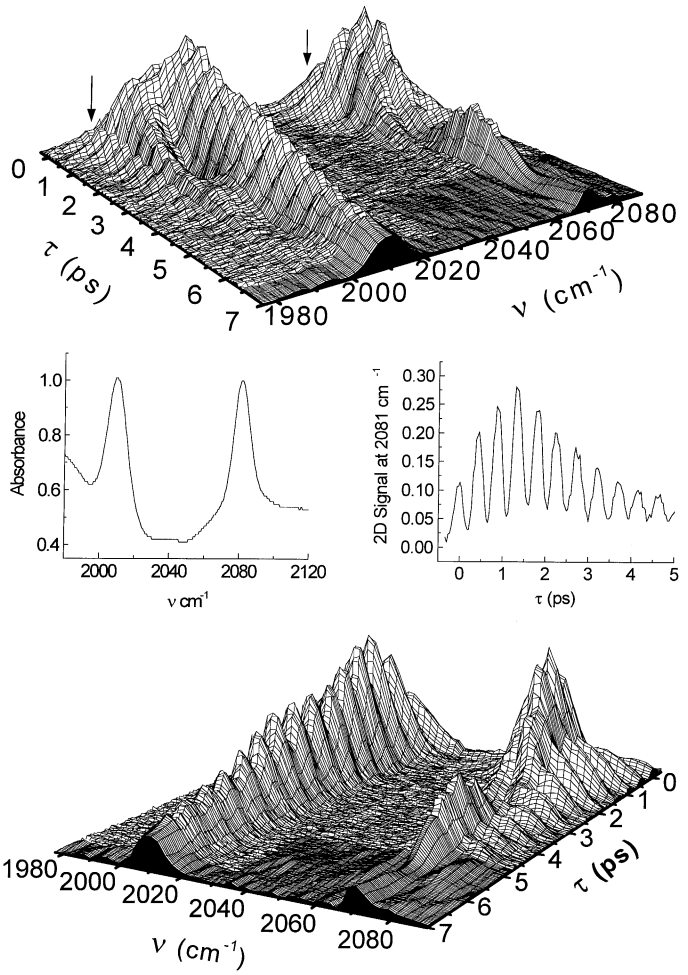

Fig. 1. The 2D VES of Rh(CO)2acac in DBP at 150 K. The upper (lower) plot displays the VES spectrum from the red (blue) side. (Point spacing is 2 cm^{-1} on the frequency axis and 34 fs on the time-axis. At long time, the spacing is 340 fs.) The arrows highlight the echo signal arising from coherences involving the A/S combination band. The left inset is the room temperature absorption spectrum of the sample. The right inset is a time-slice of the 2D VES spectrum (the monochromator wavelength set at 2081 cm^{-1}) that shows the oscillations arising from quantum beating between the A and S modes.

The various contributions to the VES have been described [9] and will be discussed in detail subsequently [19]. The blue side of each band arises from the $v = 0$–1 transition. Further to the red is a contribution from the $v = 1$–2 transition [9]. On the red edge of each band (marked by arrows) is a contribution from the coherences that involve the A/S combination band transitions [19]. The center portions of the A and S bands display a slow oscillation. This oscillation is at the frequencies of the anharmonic shift between the 0–1 and 1–2 transitions [2,9,20]. The correct mechanism for the generation of the oscillations was given recently [9]. The high frequency oscillations are a quantum beat associated with the $v = 0$–1 transitions of the A and S lines [9]. The high frequency oscillations will be used to obtain information on solute–solvent interactions that are responsible for inhomogeneous broadening.

The decay of the spectrum reflects the homogeneous dephasing of the system. The decay of the 0–1 portions of the A and S bands are almost

identical and yield a $T_2 = 16$ ps, which is in accord with previous measurements [17]. The homogeneous linewidths ($1/\pi T_2$) are $2/3$ cm^{-1} while the absorption linewidths are >10 cm^{-1} (see below), demonstrating that at the experimental temperature (150 K), the system is massively inhomogeneously broadened.

For the 0–1 transitions of the A and S lines (blue sides of the bands), the high frequency oscillations are caused by a quantum beat between the A and S mode frequencies. The center-to-center splitting of the A and S modes is 72 cm^{-1}. This is the nominal beat frequency (inset of Fig. 1). For example, for one pair of diagrams that give rise to beats in the 0–1 transitions, the density matrix evolves as

$$\rho_{00}(0) \rightarrow \rho_{0A}(\omega_A) \rightarrow \rho_{AA}(0) \rightarrow \rho_{A0}(-\omega_A)$$

and

$$\rho_{00}(0) \rightarrow \rho_{0S}(\omega_S) \rightarrow \rho_{00}(0) \rightarrow \rho_{A0}(-\omega_A),$$

where the subscripts A and S stand for the first vibrational excited states of the A and S modes, the arrows represent interactions with the radiation field, and the negative frequency represents rephasing. The two paths dephase at different frequencies because the first interactions with the radiation field in the two paths involve distinct vibrationally excited states, but the two paths rephase at the same frequency. The difference in the dephasing frequencies produces a beat in the vibrational echo signal at the frequency difference. This is a standard quantum beat that arises from a branching transition [9,21,22].

The S and A lines in the absorption spectrum are separated by 72 cm^{-1} (see inset Fig. 1). This splitting would give rise to a quantum beat at ~72 cm^{-1} in the 0–1 portion of the S and A VES bands. However, careful analysis of time-slices through the data reveals that the period of the S/A quantum beats vary for different observation wavelengths [19]. Analysis is restricted to the blue sides of the S and A lines to avoid complications of the overlapping overtone and combination band portion of the peaks. Table 1 lists the beat frequencies for a number of observation wavelengths moving progressively to the blue on the blue sides of the S and A lines. The beat frequency gradually decreases as the wavelength of observation is shortened. These observations are inconsistent with a simple picture in which the beat frequency is determined by the S/A peak-to-peak frequency difference. As the wavelength of observation within the inhomogeneous lines is changed, the beat frequency changes.

Table 1
Experimental observation wavelengths and beat frequencies

Spectral Band	Observation wavelength (cm^{-1})	Beat frequency[a] (cm^{-1})
S	2081	71.3
S	2083	70.8
S	2085	70.6
S	2087	70.3
A	2011	70.8
A	2013	70.3
A	2015	69.8
A	2017	69.4

[a] The errors on the beat frequencies are estimated to be ±0.1.

To understand the trend in the beat frequencies as the observation wavelength is varied, it is necessary to consider the nature of the solute–solvent interactions that give rise to the inhomogeneous broadening of the S and A bands. Because the CO stretches in $Rh(CO)_2acac$ are inhomogeneously broadened when dissolved in DBP at 150 K, which wavelength(s) in the A line will be associated with a given wavelength in the S line to produce a quantum beat is not immediately obvious.

Only those molecules that emit at a frequency within the monochromator's band pass will be detected. A molecule that emits at a particular S wavelength within the monochromator band pass will be observed regardless of the value of the corresponding A wavelength, resulting in a beat at the frequency $(\omega_{S^o} - \omega_{A_{S^o}})$, where ω_{S^o} is the S frequency observed by the monochromator and $\omega_{A_{S^o}}$ is the associated A frequency. The monochromator detects the subensemble of molecules that emit at ω_{S^o}, which, in principle, can have a variety of associated A frequencies. The observed signal could contain a range of beat frequencies. The amplitude of a particular beat frequency is determined by the probability of having a molecule emitting at ω_{S^o} with an associated A frequency, $\omega_{A_{S^o}}$. Then, the beat frequency observed

by the monochromator at ω_{S^o} is related to the average $\omega_{A_{S^o}}$. The functional form of the beat is the Fourier transform of the distribution of $(\omega_{S^o} - \omega_{A_{S^o}})$. If the distribution is narrow or a single value, the beat will be long lived.

To understand the beat frequency as a function of the observation wavelength, we employ a simple model that is sufficiently robust to contain the necessary elements of the problem. The details will be described subsequently [19]. The system is considered in terms of the two CO local stretching modes, α and β, with frequencies ω_α and ω_β. The local oscillators are coupled to the solvent and to each other. The coupling of the local modes to the solvent gives rise to identical Gaussian distributions of local mode frequencies centered at frequency ω_o with S.D., σ. The local modes are taken to be harmonic oscillators that are coupled by an augmented bilinear coupling term [19]. The transition frequencies from the ground state to the A and S states are $\Omega_A = (E_A - E_0)/\hbar$ and $\Omega_S = (E_S - E_0)/\hbar$, respectively. These are given by

$$\Omega_A = \tfrac{1}{2}(\omega_\alpha + \omega_\beta - \delta), \tag{1a}$$

$$\Omega_S = \tfrac{1}{2}(\omega_\alpha + \omega_\beta + \delta) \tag{1b}$$

with

$$\delta = \left[\frac{\gamma^2}{\mu^2 \omega_\alpha e^{a(\omega_\alpha - \omega_o)} \omega_\beta e^{a(\omega_\beta - \omega_o)}} + (\omega_\alpha - \omega_\beta)^2 \right]^{1/2}. \tag{2}$$

μ is the reduced mass of the CO oscillator and γ is a constant that sets the magnitude of the coupling between the two local oscillators. Bilinear coupling inherently gives rise to δ values that depend on the frequencies of the local oscillators through the ω_α and ω_β that appear in the denominator of Eq. (2) [19]. The bilinear coupling model does not produce a strong enough frequency dependent δ to reproduce the absorption spectrum line shapes. In going from the gas phase to the condensed phase, the absorptions red shift, but the S/A splitting increases [19]. (The gas phase A and S peaks are located at 2026.6 and 2091.0 cm^{-1}, respectively.) The exponentials in the denominator of Eq. (2) are a heuristic augmentation of bilinear coupling that follows the gas to condensed phase trend, that is, δ increases as the frequency is shifted to the red [19]. The parameter a, adjusts the strength of the augmentation. The A and S absorption line shapes, which are unequal, are reproduced using a small value of a (see below).

With this model, it is possible to consider several different mechanisms that can give rise to inhomogeneous broadening of the absorption bands and the effect each mechanism will have on the quantum beat frequency as a function of observation wavelength. Three models of inhomogeneous broadening are considered in terms CO local mode energies and coupling. In one, the transition energies in the S and A lines are anti-correlated either because the inhomogeneous broadening arises from variations in the coupling between the local modes or the local mode energies are anti-correlated. In the other two, the inhomogeneous distribution of local mode energies are either completely correlated or totally uncorrelated. The three cases are illustrated in Fig. 2.

In the anticorrelated case (Fig. 2a), an observation wavelength some number of S.D. to the blue of center on the S line has associated with it a wavelength on the A line the same number of S.D.

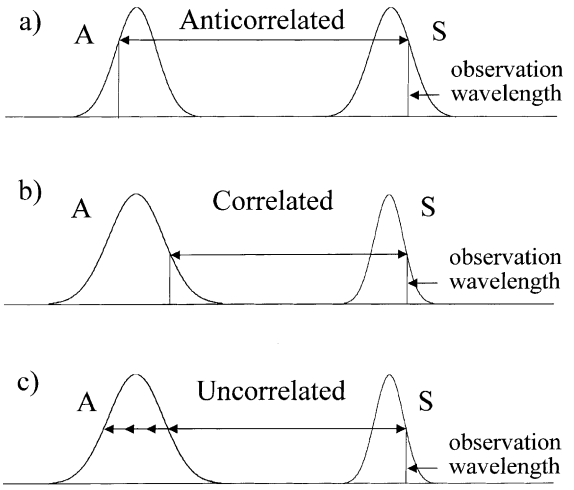

Fig. 2. Diagrams illustrating different possible scenarios that could be involved in the generation of a quantum beat at a single observation wavelength on the S line. (a) The frequencies in the A and S lines are anticorrelated. (b) The local mode frequencies are correlated. (c) The local mode frequencies are uncorrelated. Each situation gives rise to a unique prediction for the dependence of the beat frequency on observation wavelength.

the red of center. In the DBP solvent, the A/S splitting is 72 cm^{-1}. The absorption spectrum of $Rh(CO)_2acac$ in the gas phase yields a gas phase splitting of 64.4 cm^{-1}. Therefore, interaction with the solvent shifts the peaks to the red (lower energy), but it increases the splitting. The simplest manner in which the positions of the transitions in the inhomogeneously broadened S and A lines can be anticorrelated is if the solute–solvent intermolecular interactions act only to change the strength of the coupling between the two local modes. In this case, $\omega_\alpha = \omega_\beta = \omega_o$, that is, the local mode frequencies are independent of the solvent environment. Variations in the coupling parameter, γ, about an average value in the solvent, γ_o, will produce inhomogeneous broadening and will result in transition frequencies in the A and S lines that are anticorrelated. For any molecule, as γ increases, the transition frequency in the A line moves to the red, and the transition frequency in the S line moves to the blue. As the wavelength of observation in the S line is moved to the blue, the corresponding transition in the A line for the molecules under observation will move to the red. The frequency of the quantum beat, ν_b, is $\nu_b = \omega_S - \omega_A$. Therefore, as the wavelength of observation moves further to the blue on the S line, the beat frequency should increase. This is in contrast to the observed decrease in the beat frequency shown in Table 1. Calculated results are given in Table 2. Anticorrelation can also occur if the local mode frequencies are anticorrelated, that is, as ω_α increases ω_β decreases the same amount, and vice versa. The result is basically the same. Anticorrelation would lead to an increase in the beat frequency as the observation wavelength on the S band is moved farther to the blue. This is in contrast to observation.

In the correlated case (Fig. 2b), $\omega_\alpha = \omega_\beta = \omega$. The transition frequencies are obtained from Eqs. (1a), (1b) and (2). The absorption spectrum shows that the A and S lines are basically Gaussian in shape, but they have different inhomogeneous widths. The widths of the A and S absorption bands are 12.6 and 10.2 cm^{-1}, respectively, at the experimental temperature, 150 K. For $\sigma = 6.85$ cm^{-1} and $a = 0.0025$, the A and S linewidths are calculated to be 12.65 and 10.20 cm^{-1}, respectively, in accord with the experimental values (see Fig. 3a). For the correlated case, the beat frequency decreases as the observation wavelength is moved further to the blue on the S line. In fact, the same parameters that reproduce the linear absorption spectrum do a reasonably good job of reproducing the trend in the beat frequency as a function of observation wavelength on the blue side of the S line. Results of the calculations are shown in Table 2.

In the uncorrelated case (Fig. 2c), for a given ω_α value, ω_β can take on any value with the probability for a particular value given by the Gaussian distribution of local mode frequencies. The tran-

Table 2
Calculated beat frequencies

Observation frequency (cm^{-1})	Anticorrelated beat frequency (cm^{-1})	Correlated beat frequency (cm^{-1})	Uncorrelated beat frequency (cm^{-1})
S line			
2072	52	74.50	70.99
2077	62	73.25	71.82
2082	72	72.00	72.60
2087	82	70.75	73.33
2092	92	69.50	73.96
A line			
2000	92	74.00	71.22
2005	82	73.00	72.00
2010	72	72.00	72.68
2015	62	71.00	73.29
2020	52	70.00	73.88

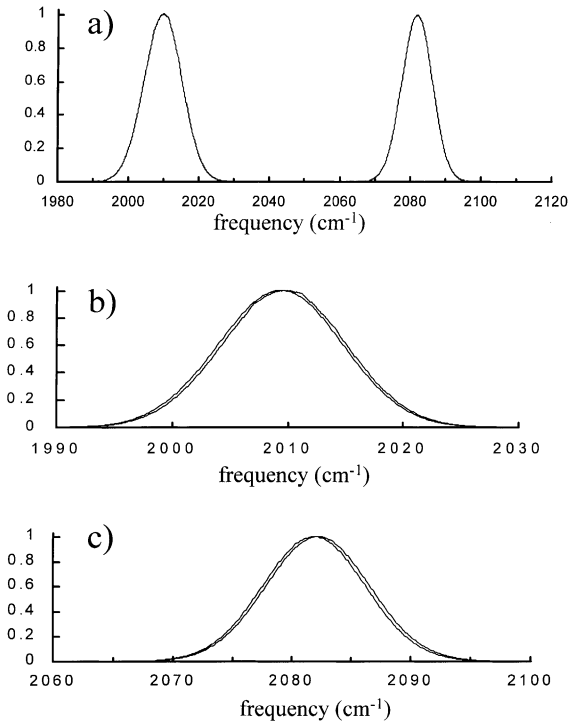

Fig. 3. The linear spectrum predicted by the augmented bilinear coupling model with parameters chosen to mimic the observed linear absorption spectrum of $Rh(CO)_2acac$ in DBP. (a) The predicted absorption spectrum assuming complete correlation of the local mode frequencies. The model is able to accurately reproduce the absorption spectrum with the correct peak splitting and linewidths. In parts (b) and (c) the predicted absorption spectrum assuming complete correlation (correlated model) is blown up and overlaid with the predicted spectrum assuming a total lack of correlation (uncorrelated model). The correlated and uncorrelated cases predict essentially identical spectra for the same input parameters.

sition frequencies are calculated using Eqs. (1a), (1b) and (2). In contrast to the correlated case, in the uncorrelated case, a range of pairs of local mode frequencies $(\omega_\alpha, \omega_\beta)$ can give rise to a particular transition frequency. The probability of having a particular pair of frequencies is $P(\omega_\alpha, \omega_\beta) = P(\omega_\alpha) \times P(\omega_\beta)$. In spite of the difference between the correlated and uncorrelated cases, the calculated linear absorption spectrum using the uncorrelated model is virtually identical to the spectrum calculated using the correlated model with the same parameters. Fig. 3b, c display the calculated absorption spectra for the A and S lines, respectively, for both the correlated and uncorrelated cases. Therefore, the correlated and uncorrelated models cannot be distinguished by comparison of the calculated line shapes with the absorption spectrum.

Consider a single S transition frequency ω_S (as would be selected for experimental observation by the monochromator). Because ω_α and ω_β can vary independently, there are many possible pairs of local mode frequencies ω_α and ω_β that give rise to a single ω_S. However, each such pair of frequencies (having probability $P(\omega_\alpha, \omega_\beta)$) corresponds to a different A transition frequency ω_A. The net result is that a single ω_S maps to a distribution of ω_A where the weight of each ω_A is given by $P(\omega_\alpha, \omega_\beta)$. Examples of this mapping distribution are shown in Fig. 4. The probability weighted spread of beat

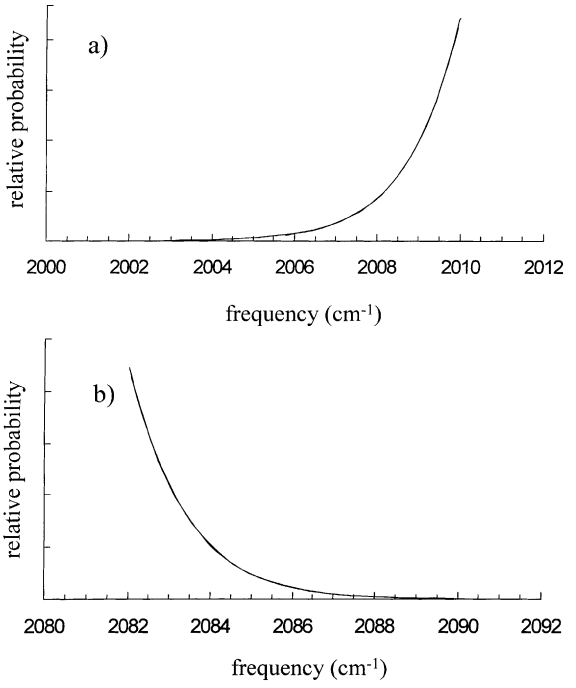

Fig. 4. For a given observation wavelength on the S (A) line the mapping onto the set of transition frequencies on the A (S) line is shown for the case of uncorrelated local mode energies. (a) S line observation wavelength is 2082 cm^{-1}. (b) A line observation wavelength is 2010 cm^{-1}. The curves are the relative probabilities. The calculations show that a single observation wavelength does not map onto a single transition frequency on the other line.

frequencies is sufficiently narrow that decay of the beats through destructive interference will not occur on the time-scale of the experiment [19]. Rather, the uncorrelated model predicts observation of a strong beat at the average beat frequency.

In Table 2, the predicted beat frequencies for the uncorrelated model are tabulated for a series of observation wavelengths. As the observation wavelength on the S line moves further to the blue, the model predicts that the beat frequency increases, which is contrary to observation.

The results of the calculations (Table 2) demonstrate that the correlated case produces the correct trend in the beat frequency with observation wavelength. The parameters that give the correct line widths and splitting of the peaks in the absorption spectrum produce the correct trend in the beat frequencies and produce changes in the beat frequency with observation that are similar but not identical to those that are observed. For example, for observation wavelengths 2082 and 2087 cm^{-1} the correlated case calculations give beat frequencies of 72.00 and 70.75 cm^{-1}, respectively. The difference is 1.25 cm^{-1}. The experimental values at these wavelengths are 71.1 and 70.3 cm^{-1}. The difference is 0.8 cm^{-1}. The other models predict incorrect trends. In a subsequent publication, possible mechanisms of solute–solvent interactions that could give rise to the observations are discussed [19].

Ultrafast infrared 2D vibrational echo spectroscopy has been used to examine solute–solvent interactions. Both the experiments and theory presented here should be taken to be preliminary. Nonetheless, it is clear that the 2D spectrum can provide information that cannot be obtained from the 1D vibrational echo experiment. The results demonstrate that new types of information can be obtained from the application of 2D vibrational echo spectroscopy to molecular systems.

Acknowledgements

This work was supported by the National Institutes of Health (1RO1-GM61137), the National Science Foundation (DMR-0088942), and AFOSR (F49620-94-1-0141). K.A.M. is supported by an Abbott Laboratories Stanford Graduate Fellowhip.

References

[1] D. Zimdars, A. Tokmakoff, S. Chen, S.R. Greenfield, M.D. Fayer, T.I. Smith, H.A. Schwettman, Phys. Rev. Lett. 70 (1993) 2718.
[2] K.D. Rector, A.S. Kwok, C. Ferrante, A. Tokmakoff, C.W. Rella, M.D. Fayer, J. Chem. Phys. 106 (1997) 10 027.
[3] K.D. Rector, C.W. Rella, A.S. Kwok, J.R. Hill, S.G. Sligar, E.Y.P. Chien, D.D. Dlott, M.D. Fayer, J. Phys. Chem. B. 101 (1997) 1468.
[4] K.D. Rector, M.D. Fayer, Int. Rev. Phys. Chem. 17 (1998) 261.
[5] P. Hamm, M. Lim, W.F. Degrado, R.M. Hochstrasser, J. Chem. Phys. 112 (2000) 1907.
[6] M.C. Asplund, M.T. Zanni, R.M. Hochstrasser, Proc. Natl. Acad. Sci. USA 97 (2000) 8219.
[7] K.D. Rector, D.E. Thompson, K. Merchant, M.D. Fayer, Chem. Phys. Lett. 316 (2000) 122.
[8] M.A. Berg, K.D. Rector, M.D. Fayer, J. Chem. Phys. 113 (2000) 3233.
[9] K.A. Merchant, D.E. Thompson, M.D. Fayer, Phys. Rev. Lett., 2001, accepted.
[10] K.D. Rector, M.D. Fayer, J.R. Engholm, E. Crosson, T.I. Smith, H.A. Schwettmann, Chem. Phys. Lett. 305 (1999) 51.
[11] K.D. Rector, D.A. Zimdars, M.D. Fayer, J. Chem. Phys. 109 (1998) 5455.
[12] W.M. Zhang, V. Chernyak, S. Mukamel, J. Chem. Phys. 110 (1999) 5011.
[13] M.C. Asplund, M. Lim, R.M. Hochstrasser, Chem. Phys. Lett. 323 (2000) 269.
[14] O. Golonzka, M. Khalil, N. Demirdoven, A. Tokmakoff, Phys. Rev. Lett. 86 (2001) 2154.
[15] M. Khalil, A. Tokmakoff, Chem. Phys., 2001, in press.
[16] K.D. Rector, M.D. Fayer, J. Chem. Phys. 108 (1998) 1794.
[17] K.D. Rector, A.S. Kwok, C. Ferrante, R.S. Francis, M.D. Fayer, Chem. Phys. Lett. 276 (1997) 217.
[18] D.E. Thompson, J.C. Wright, J. Phys. Chem. A 104 (2000) 11 282.
[19] D.E. Thompson, K.A. Merchant, M.D. Fayer, J. Chem. Phys., 2001, in preparation.
[20] P. Hamm, M. Lim, M. Asplund, R.M. Hochstrasser, Chem. Phys. Lett. 301 (1999) 167.
[21] A.I. Lvovsky, S.R. Hartmann, Laser Phys. 6 (1996) 535.
[22] M. Koch, J. Feldmann, G. von Plessen, E.O. Gobel, P. Thomas, K. Kohler, Phys. Rev. Lett. 69 (1992) 3631.